The Astrophysical Journal Supplement Series, 215:5 (16pp), 2014 November doi:10.1088/0067-0049/215/1/5

CONSTRAINTS ON THE MINIMUM ELECTRON LORENTZ FACTOR AND MATTER CONTENT OF JETS FOR A SAMPLE OF BRIGHT *FERMI* BLAZARS

Shi-Ju Kang[1], Liang Chen[2], and Qingwen Wu[1,3]
[1] School of Physics, Huazhong University of Science and Technology, Wuhan 430074, China; qwwu@hust.edu.cn
[2] Key Laboratory for Research in Galaxies and Cosmology, Shanghai Astronomical Observatory, Chinese Academy of Sciences, 80 Nandan Road, Shanghai 200030, China
Received 2014 May 8; accepted 2014 September 8; published 2014 October 20

ABSTRACT

We fit (quasi-)simultaneous multi-waveband spectral energy distributions for a sample of low-synchrotron-peaked (LSP) blazars with a one-zone leptonic model. The seed photons that predominantly come from the broad line region (BLR) and infrared (IR) molecular torus are considered in the context of an external Compton process. We find that modeling with IR seed photons is systematically better than that with BLR photons based on a χ^2 test, which suggests that γ-ray-emitting regions are most likely found outside the BLR. The minimum electron Lorentz factor, $\gamma_{\rm min}$, is constrained from the modeling of these LSP blazars with good soft X-ray data (ranging from 5 to 160 with a median value of 55), which plays a key role in jet power estimation. Assuming a one-to-one ratio of protons to electrons, we find that the jet power for LSP blazars is systematically higher than that of FR II radio galaxies at a 151 MHz radio luminosity, $L_{151\,\rm MHz}$ even though FR IIs are regarded as the same as LSP blazars in a unification scheme except at the jet viewing angle. A possible reason for this is that there are some $e^{\pm}$ pairs in the jets of these blazars. If this is the case, we find that the number density of $e^{\pm}$ pairs should be several times higher than that of e^{-}–p pairs by assuming the jet power is the same for LSP blazars and FR IIs at the given $L_{151\,\rm MHz}$.

Key words: BL Lacertae objects: general – galaxies: jets – plasmas – quasars: general – radiation mechanisms: non-thermal

Online-only material: color figures

1. INTRODUCTION

Blazars are the most extreme and powerful sources among active galactic nuclei (AGNs) and their broadband emission is mainly dominated by non-thermal components produced in a relativistic jet pointing toward us (Urry & Padovani 1995). Blazars are traditionally sub-divided into flat spectrum radio quasars (FSRQs) and BL Lacertae objects (BL Lacs) according to their emission-line features, with BL Lacs having weak or no emission lines (e.g., the equivalent width, EW, of the emission line in the rest frame is less than 5 Å) and FSRQs having stronger emission lines (EW $\geqslant$ 5 Å; e.g., Urry & Padovani 1995). The different emission-line properties of FSRQs and BL Lacs may be triggered by accretion mode transition, where a standard cold accretion disk (e.g., Shakura & Sunyaev 1973) exists in FSRQs while advection-dominated accretion flow (e.g., Narayan & Yi 1994, 1995) exists in BL Lacs (e.g., Ghisellini & Celotti 2001; Wang et al. 2002; Cao 2003; Wu & Cao 2006; Xu et al. 2009). The spectral energy distribution (SED) of blazars generally exhibits a two-bump structure. The lower energy bump is commonly ascribed to synchrotron radiation and peaks at infrared to X-ray bands, while the higher energy bump, attributed to inverse Compton (IC) scattering, peaks at MeV–GeV bands. The location of the peak for the lower energy bump in the SED, $\nu_{\rm p}^{\rm S}$, is also used to classify the sources as low-synchrotron-peaked (LSP; e.g., $\nu_{\rm p}^{\rm S} < 10^{14}$ Hz), intermediate-synchrotron-peaked (ISP; e.g., 10^{14} Hz $< \nu_{\rm p}^{\rm S} < 10^{15}$ Hz), and high-synchrotron-peaked (HSP; e.g., $\nu_{\rm p}^{\rm S} > 10^{15}$ Hz) blazars (e.g., Padovani & Giommi 1995; Abdo et al. 2010). In contrast to BL Lac objects, all FSRQs are essentially LSP blazars.

The origin of the seed photons for IC scattering in blazars is uncertain, but possible locations for their origin include synchrotron photons (synchrotron self-Compton, SSC, process; Marscher & Gear 1985; Maraschi et al. 1992) and/or external photons (external-Compton, EC, process), where the external photons could possibly originate from the accretion disk (e.g., Dermer & Schlickeiser 1993), the broad line region (BLR; e.g., Sikora et al. 1994; Fan et al. 2006), and/or the molecular torus (e.g., Blazejowski et al. 2000; Arbeiter et al. 2002; Sokolov & Marscher 2005). Normally, the SEDs of HSP blazars (e.g., BL Lacs) seem to be consistent with pure SSC models (e.g., Mastichiadis & Kirk 1997; Krawczynski et al. 2004; Zhang et al. 2014), while the LSP blazars often require an EC component to explain their γ-ray spectra (e.g., Sambruna et al. 1999; Böttcher & Chiang 2002; Chen & Bai 2011; Yan et al. 2014). No EC process in BL Lacs is caused by the disappearance of the BLR (e.g., Tran 2001; Gu & Huang 2002; Laor 2003; Elitzur & Ho 2009; Cao 2010) and/or torus (e.g., Hönig & Beckert 2007; Ho 2008) in the low-power sources. Identifying the origin of external seed photons in FSRQs is also a diagnostic for the location of the γ-ray-emitting region (e.g., Agudo et al. 2011). For example, the external seed photons will dominantly originate from the cold disk if the γ-ray-emitting region is less than several hundreds ($R_{\rm S}$) from the central black hole (BH), while the soft photons will mainly come from the BLR if the γ-ray-emitting region is larger than several hundred times the size of the $R_{\rm S}$ and less than several thousand times the size of the $R_{\rm S}$. If the γ-ray-emitting region remains outside the BLR and less than $\sim 10^5 R_{\rm S}$, the most abundant seed photons are IR photons coming from the molecular torus. Cosmic background photons may be important if the γ-ray-emitting region is much larger than $\sim 10^5 R_{\rm S}$ (see Figures 2 and 3 in Ghisellini & Tavecchio 2009).

[3] To whom any correspondence should be addressed.

The content of jet matter is also a mystery, which could possibly include a "normal" plasma of protons and relativistic electrons (an e^{-}–p jet), a "pair" plasma consisting only of relativistic electrons and positrons (an $e^{\pm}$ jet), or a combination of the two. Distinguishing between these possibilities is crucial for understanding the physical processes of a jet occurring close to the central engine. Several methods for exploring this issue have been proposed. One method is based on synchrotron self-absorption (SSA) arguments combined with the total kinetic power of jets (e.g., Reynolds et al. 1996; Hirotani 2005), where the measurements on the flux and the size of the radio core lead to constraints on the number density of relativistic electrons and the magnetic field strength in a jet. Using this method, Reynolds et al. (1996) concluded that the core of M 87 is probably dominated by an $e^{\pm}$ plasma. A second method is the constraint from circular polarization in the radio core, which is due to the Faraday conversion of linear to circular polarization caused by low-energy electrons. Wardle et al. (1998) suggested that the jet of 3C 279 is composed mainly of $e^{\pm}$ pairs based on its small minimum Lorentz factor of electrons ($\gamma_{\rm min} \sim 1$) which are derived from the circular polarizations of the radio core. A third constraint comes from the cocoon dynamics of the jets. Kino et al. (2012) suggested that the jet of Cygnus A should be dominated by a mixed composition of e^{-}–e^{+}–p by comparing the partial pressures of electrons and protons with the observational pressure of a cocoon estimated from the interaction between a jet and the interstellar medium. A fourth approach is the constraint from the absence of bulk-Compton emission in FSRQs (e.g., Sikora & Madejski 2000; Ghisellini & Tavecchio 2010), where the electrons in the jet traveling with a bulk Lorentz factor Γ interact with the photons produced by the accretion disk and/or broad emission lines and radiate at soft X-rays. Kataoka et al. (2008) and Ghisellini (2012) argue against the pure $e^{\pm}$ pair jets based on the absence of observational features of soft X-ray excess.

Jet power is important for understanding jet formation, the disk–jet relation, the jet kinetic luminosity function, and jet feedback (e.g., Blandford & Sikora 1987; Lei et al. 2005, 2008; Spruit 2010; Narayan & McClintock 2012; Li & Cao 2012; Wu et al. 2013; Cao & Spruit 2013; Cao 2014). The X-ray cavities in galaxy clusters and giant elliptical galaxies provide a direct measurement of the mechanical energy released by the AGN jets through the work done on the hot, gaseous halos surrounding them (i.e., Fabian et al. 2000; Bîrzan et al. 2004; Allen et al. 2006; Rafferty et al. 2006; Bîrzan et al. 2008; Cavagnolo et al. 2010; Wu et al. 2011). The jet power of FR II radio galaxies and radio quasars can be estimated directly from the measurements of the hotspot size and equipartition magnetic field strength along with some assumptions (i.e., Godfrey & Shabala 2013). Celotti et al. (1993) estimated the jet power from the number of emitting particles, magnetic field strength, and jet velocity constrained by the radio and X-ray data using the standard SSC theory (see also Tavecchio et al. 2007; Celotti & Ghisellini 2008; Gu et al. 2009). Modeling the multi-waveband SEDs of blazars also returns the particle number, magnetic field strength, and Doppler factor of the jet where the kinetic jet power can also be derived with some reasonable assumptions (i.e., Maraschi et al. 2003; Celotti & Ghisellini 2008; Ghisellini et al. 2009; Zhang et al. 2014). It should be noted that the last two methods suffer from uncertainties on the jet matter content and the low-energy cutoff, $\gamma_{\rm min}$, of electrons, where the parameter $\gamma_{\rm min}$ is coupled with the parameter of the electron number density (i.e., Celotti et al. 1993). The value of $\gamma_{\rm min}$ can be strongly constrained in some LSP blazars (e.g., FSRQs) if their soft X-ray emission is dominated by the SSC process (i.e., Tavecchio et al. 2007; Celotti & Ghisellini 2008; Zhang et al. 2014).

In this work, we explore the issue of possible external seed photon fields (e.g., BLR or IR torus) for a sample of LSP blazars using a χ^2 test in the SED modeling (Mankuzhiyil et al. 2011; Zhang et al. 2012, 2014). The parameter $\gamma_{\rm min}$ can be constrained for these LSP blazars with good quality of soft X-ray data in the SED modelings. We further investigate the issue of jet power and jet matter content if the $\gamma_{\rm min}$ is known. The sample is described in Section 2. Section 3 contains detailed information about our model. We present the results in Section 4. The last section was devoted to discussion and conclusion. Throughout this work, we assume the following cosmology: $H_0 = 70$ km s^{-1} Mpc^{-1}, $\Omega_0 = 0.3$ and $\Omega_\Lambda = 0.7$.

2. THE SAMPLE

For the purpose of this work, we select 28 LSP blazars with $\nu_{\rm p}^{\rm S} < 10^{14}$ Hz from Giommi et al. (2012), where the broadband SEDs from radio to γ-rays are available based on (quasi-)simultaneous observations of *Plank, Swift, Fermi* and some ground-based telescopes. The data from radio to X-rays for these blazars are simultaneous. For the γ-ray data, Giommi et al. (2012) presented simultaneous observations accumulated during the *Plank* observation, quasi-simultaneous observations integrated over a period of 2 months centered on the *Plank* observation, and 27 months of *Fermi*-LAT integration from 2008 August 4 to 2010 November 4. The SEDs of these sources are presented in Figures 9–14 where the simultaneous and quasi-simultaneous γ-ray data are shown with circles and squares, respectively, while the triangles represent the *Fermi* data integrated over 27 months. Two γ-ray loud LSP blazars (PKS 1502+036 and PKS 2004−447) with quasi-simultaneous broadband SEDs from IR to γ-rays were also selected from Paliya et al. (2013). In total, our sample includes 30 sources. Detailed information about the sample is presented in Table 1. We present the LAT name and a counterpart name in Columns 1 and 2, respectively. The redshift is shown in Column 3. We search the literature for minimum variability timescales of individual objects and finally find the optical and/or γ-ray data for 11 sources (Böttcher et al. 2007; Vovk & Neronov 2013; Liang & Liu 2003), which are reported in Column 4. To compare our modeling parameters, the Doppler factors estimated from variability brightness temperatures are also listed in Column 5 for 15 sources, which are selected from Savolainen et al. (2010). The model parameters constrained from the SED fittings are shown in Columns 6–14. Column 15 shows the adopted γ-ray data in the modeling where we prefer to use the simultaneous data, then use the quasi-simultaneous data if the amount of simultaneous data is less than three, and the integrated data within 27 months is our last choice if the quasi-simultaneous data are also less than three.

3. THE MODEL

We adopt a relatively simple, one-zone, homogeneous synchrotron and IC model, which is widely used in to model the SED of blazars (e.g., Ghisellini et al. 2010, and references therein). The emitting plasma is assumed to be a spherical region with a radius of R. A Doppler factor of $\delta = [\Gamma(1-\beta\cos\theta)]^{-1} \approx \Gamma$ is assumed for the relativistic jet close to the line of sight in blazars with a viewing angle

Table 1
The Parameters Used to Model the SED

					IR								BLR	
J2000.0 Name	Source Name	z	$t_{\rm var}$	$\delta_{\rm var}$[a]	B (G)	δ	$\gamma_{\rm min}$	$\gamma_{\rm b}(10^3)$	p_1	p_2	$N_0(10^4)$	χ^2	χ^2	Data[b]
(1)	(2)	(3)	(4)	(5)	(6)	(7)	(8)	(9)	(10)	(11)	(12)	(13)	(14)	(15)
J0136+4751	S4 0133+47	0.859	...	20.5	1.09 ± 0.24	27.01 ± 1.93	8.34 ± 3.94	0.28 ± 0.06	1.99 ± 0.06	4.05 ± 0.19	0.08 ± 0.03	0.62	1.43	B
J0237+2848	4C 28.7	1.213	...	16.0	0.99 ± 0.14	27.98 ± 1.16	7.42 ± 3.56	0.69 ± 0.09	2.16 ± 0.04	4.12 ± 0.15	0.09 ± 0.02	0.24	0.43	B
J0334−4008	PKS 0332−403	1.445	...	...	0.72 ± 0.15	24.38 ± 2.16	89.18 ± 74.29	1.09 ± 0.29	2.51 ± 0.06	4.42 ± 0.39	4.78 ± 1.63	0.52	1.44	B
J0457−2324	PKS 0454−234	1.003	0.78[c]	...	0.51 ± 0.11	26.03 ± 1.25	$17.83^{+60.96}_{-15.83}$	0.42 ± 0.10	2.44 ± 0.04	3.58 ± 0.12	2.60 ± 0.64	0.34	0.46	A
J0522−3627	PKS 0521−36	0.057	0.43[c]	...	0.93 ± 0.04	9.67 ± 0.19	47.54 ± 13.73	1.59 ± 0.10	2.35 ± 0.01	4.51 ± 0.12	21.05 ± 1.18	0.03	0.23	B
J0538−4405	PKS 0537−441	0.894	0.53[d]	...	1.49 ± 0.28	35.60 ± 2.64	62.09 ± 36.38	0.57 ± 0.15	2.32 ± 0.05	3.83 ± 0.31	1.22 ± 0.27	0.50	2.22	A
J0854+2006	OJ 287	0.306	1.49[c]	16.8	1.94 ± 0.28	14.82 ± 0.81	63.74 ± 61.21	0.75 ± 0.14	2.00 ± 0.03	3.65 ± 0.14	1.29 ± 0.26	0.32	0.63	B
J1058−0133	4C 1.28	0.890	...	12.1	0.95 ± 0.08	20.44 ± 0.63	52.61 ± 35.56	0.52 ± 0.06	2.22 ± 0.02	3.98 ± 0.10	1.23 ± 0.14	0.09	0.68	B
J1130−1449	PKS 1127−145	1.184	...	...	1.40 ± 0.13	18.74 ± 0.66	84.05 ± 42.16	0.58 ± 0.07	2.01 ± 0.02	3.98 ± 0.12	0.83 ± 0.09	0.10	0.62	C
J1159+2914	4C 29.45	0.725	0.29[d]	28.2	0.81 ± 0.19	32.50 ± 1.97	79.05 ± 55.27	0.29 ± 0.08	2.54 ± 0.05	3.70 ± 0.16	10.31 ± 2.89	0.34	1.35	A
J1222+0413	PKS 1219+04	0.965	...	...	0.99 ± 0.09	20.47 ± 0.73	162.64 ± 18.42	0.52 ± 0.05	1.96 ± 0.02	4.40 ± 0.14	0.46 ± 0.04	0.07	0.84	B
J1229+0203	3C 273	0.158	0.58[c]	16.8	1.13 ± 0.11	11.68 ± 0.39	37.09 ± 22.84	1.52 ± 0.16	2.08 ± 0.01	4.15 ± 0.14	11.20 ± 0.98	0.07	0.16	A
J1256−0547	3C 279	0.533	2.00[e]	23.8	0.48 ± 0.04	19.36 ± 0.68	84.55 ± 39.05	0.81 ± 0.06	2.17 ± 0.02	5.01 ± 0.13	0.50 ± 0.06	0.14	0.37	A
J1505+0326	PKS 1502+036	0.408	...	...	0.45 ± 0.04	12.28 ± 0.45	47.66 ± 41.13	1.84 ± 0.21	2.21 ± 0.02	4.31 ± 0.20	1.28 ± 0.19	0.14	0.19	A
J1517−2422	AP Lib	0.049	...	...	0.50 ± 0.10	7.72 ± 0.06	$47.25^{+118.63}_{-45.25}$	1.90 ± 0.33	1.59 ± 0.04	4.41 ± 0.36	0.09 ± 0.02	0.49	0.79	B
J1642+3948	3C 345	0.593	...	7.7	0.60 ± 0.09	21.10 ± 1.18	$21.71^{+33.72}_{-19.71}$	0.80 ± 0.17	2.53 ± 0.03	4.11 ± 0.21	5.06 ± 0.99	0.31	1.03	A
J1800+7828	S5 1803+784	0.680	1.03[c]	12.1	0.93 ± 0.11	18.73 ± 0.94	61.91 ± 49.93	1.14 ± 0.16	2.03 ± 0.03	4.23 ± 0.20	0.29 ± 0.05	0.23	0.77	A
J1833−2103	PKSB 1830−210	2.507	0.32[c]	...	0.54 ± 0.20	53.90 ± 3.73	4.92 ± 1.82	0.47 ± 0.11	2.27 ± 0.08	4.45 ± 0.32	0.94 ± 0.34	0.63	1.98	A
J1911−2006	PKSB 1908−201	1.119	...	...	0.39 ± 0.06	28.27 ± 0.82	17.68 ± 5.28	0.26 ± 0.03	2.20 ± 0.03	4.21 ± 0.08	0.80 ± 0.12	0.05	0.49	B
J1923−2104	PMNJ 1923-2104	0.874	...	...	1.01 ± 0.10	20.90 ± 0.84	56.91 ± 26.48	1.29 ± 0.19	2.20 ± 0.02	4.03 ± 0.23	0.67 ± 0.08	0.12	0.57	B
J2007−4434	PKS 2004−447	0.048	...	...	0.45 ± 0.03	9.05 ± 0.27	47.78 ± 21.96	2.65 ± 0.20	2.26 ± 0.01	5.52 ± 0.36	4.27 ± 0.37	0.09	0.05	A
J2148+0657	4C 6.69	0.990	...	15.5	0.78 ± 0.11	18.79 ± 0.83	12.42 ± 4.53	0.46 ± 0.08	2.28 ± 0.02	4.59 ± 0.23	4.42 ± 0.55	0.11	1.14	C
J2151−3027	PKS 2149−307	2.345	...	...	1.10 ± 0.07	18.03 ± 0.43	160.98 ± 13.89	0.99 ± 0.09	2.24 ± 0.01	4.34 ± 0.12	12.95 ± 0.81	0.03	0.35	C
J2202+4216	BL Lac	0.069	1.06[c]	7.2	0.70 ± 0.06	8.17 ± 0.27	$10.51^{+60.16}_{-8.51}$	1.77 ± 0.21	2.22 ± 0.02	3.74 ± 0.12	3.60 ± 0.45	0.13	0.19	A
J2203+3145	4C 31.63	0.295	...	6.6	0.83 ± 0.12	12.03 ± 0.41	5.43 ± 4.98	0.79 ± 0.14	2.31 ± 0.02	4.44 ± 0.24	5.70 ± 0.62	0.07	0.38	C
J2207−5346	PKS 2204−54	1.206	...	...	1.44 ± 0.23	18.41 ± 1.04	123.51 ± 57.21	0.92 ± 0.18	2.49 ± 0.04	4.17 ± 0.21	6.49 ± 1.52	0.24	1.02	C
J2229−0832	PKS 2227−08	1.560	...	15.8	0.99 ± 0.13	24.96 ± 1.31	111.23 ± 42.56	0.51 ± 0.09	2.45 ± 0.03	4.12 ± 0.17	4.35 ± 0.75	0.21	1.36	B
J2232+1143	4C 11.69	1.037	0.45[d]	15.5	1.01 ± 0.22	24.98 ± 1.11	88.67 ± 37.43	0.63 ± 0.12	2.49 ± 0.03	4.19 ± 0.17	13.76 ± 2.24	0.15	1.19	C
J2253+1608	3C 454.3	0.859	...	32.9	0.85 ± 0.20	32.98 ± 2.08	87.89 ± 51.45	0.42 ± 0.08	2.07 ± 0.04	4.26 ± 0.23	0.74 ± 0.17	0.55	2.21	A
J2327+0940	PKS 2325+093	1.843	...	...	0.86 ± 0.11	25.08 ± 1.21	165.99 ± 35.98	0.40 ± 0.05	2.06 ± 0.03	4.17 ± 0.14	0.81 ± 0.12	0.16	0.75	C

Notes.

[a] The Doppler factor derived from the radio variability, which is selected from Savolainen et al. (2010).

[b] The adopted γ-ray data in the modeling, where A represents the simultaneous data, B represents quasi-simultaneous data, and C represents the integrated data within 27 months.

[c] The minimum γ-ray variability timescale selected from Vovk & Neronov (2013).

[d] The minimum optical variability timescale selected from Liang & Liu (2003).

[e] The minimum optical variability timescale selected from Böttcher et al. (2007).

of $\theta \lesssim 1/\Gamma$. The electron spectrum is described by a broken power-law distribution with the form

$$N(\gamma) = \begin{cases} N_0 \gamma^{-p_1} & \gamma_{\rm min} \leqslant \gamma \leqslant \gamma_{\rm b} \\ N_0 \gamma_{\rm b}^{p_2-p_1} \gamma^{-p_2} & \gamma_{\rm b} < \gamma \leqslant \gamma_{\rm max}, \end{cases} \quad (1)$$

where γ_b is the broken electron Lorentz factor, p_1 and p_2 represent the indices of the electron distribution below and above γ_b, the parameters $\gamma_{\rm min}$ and $\gamma_{\rm max}$ are the minimum and maximum electron Lorentz factors, and N_0 is the normalization of the particle distribution.

Both SSC and EC are included in our calculation, where the Klein–Nishina (KN) effect is properly considered in the IC scattering (see Rybicki & Lightman 1979; Blumenthal & Gould 1970). In the EC mechanism, we assume that the seed photons predominantly originate from the BLR and molecular torus, respectively. For the dissipation region within the BLR (e.g., $R_{\rm diss} \lesssim R_{\rm BLR}$), the seed photon energy density is $u_{\rm BLR} \sim f_{\rm BLR} L_{\rm d}/(4\pi c R_{\rm BLR}^2)$, where $f_{\rm BLR} \sim 0.1$ is the fraction of the disk luminosity, $L_{\rm d}$, that is re-emitted by the broad lines. The reverberation mapping indicated that the typical size of BLR is $R_{\rm BLR} = 10^{17} L_{\rm d,45}^{1/2}$ cm (e.g., Kaspi et al. 2007; Bentz et al. 2009), which implies that the energy density of the soft photons from BLR is roughly constant with $u_{\rm BLR} = 2.65 \times 10^{-2}$ erg cm^{-3}. In the jet comoving frame, $u'_{\rm BLR} = (17/12)\,\Gamma^2 u_{\rm BLR}$ (see Ghisellini & Tavecchio 2008; Ghisellini & Tavecchio 2009, for details). The radiation from BLR is taken as an isotropic blackbody with a peak frequency of $2 \times 10^{15}\Gamma$ Hz mainly contributed by Lyα lines (Ghisellini & Tavecchio 2008). For the case of $R_{\rm diss} > R_{\rm BLR}$, the photon field from BLR will decrease quickly (e.g., Ghisellini & Tavecchio 2009) and the seed photons should mainly come from the molecular torus. Similar to $u_{\rm BLR}$, $u_{\rm IR} \sim f_{\rm IR} L_{\rm d}/(4\pi c R_{\rm IR}^2)$, where $R_{\rm IR} = 2.5 \times 10^{18} L_{\rm d,45}^{1/2}$ cm and $f_{\rm IR} \sim 0.5$ (Ghisellini & Tavecchio 2008). In the jet comoving frame, $u'_{\rm IR} = 3 \times 10^{-4}\Gamma^2$ erg cm^{-3} (Cleary et al. 2007). The radiation from the reprocessed torus is described as a blackbody spectrum with a peak frequency of $\nu_{\rm IR} = 3 \times 10^{13}$ Hz in the lab frame, which is roughly independent of the disk luminosity since $R_{\rm IR}$ scales as $L_{\rm d}^{1/2}$ (Cleary et al. 2007).

There are nine parameters in our model: R, B, δ, p_1, p_2, $\gamma_{\rm min}$, $\gamma_{\rm max}$, $\gamma_{\rm b}$, and N_0. Instead of the more commonly used "eyeball" fit, we employ a χ^2-minimization procedure to constrain the free parameters. However, it will take too long to get the best fit if we allow all nine parameters to be free. In this work, we estimate the size of the emitting region from the minimum variability timescale $\Delta t_{\rm var}$, which is obtained from $R = c\delta\Delta t_{\rm var}/(1+z)$, where c is the speed of light and z is the redshift. $\Delta t_{\rm var}$ values for optical/γ-rays for 11 sources are collected from the literature with an average value of $\langle \Delta t_{\rm var} \rangle \simeq 0.82$ day. For the sources with no reported minimum variability timescales, the typical value of 1 day will be adopted (e.g., Ghisellini et al. 1998; Abdo et al. 2009; Fossati et al. 2008; Zhang et al. 2012; Cao & Wang 2013). The model is not sensitive to the parameter $\gamma_{\rm max}$ and we set $\gamma_{\rm max} = 100\gamma_{\rm b}$ in this work which will not affect our results. Therefore, there are seven free parameters in our SED fittings. For a given source, we generate all the parameters in a broad range and calculate the reduced χ^2 for these parameters. Then we derive a probability distribution of χ^2 (e.g., $p \propto \exp(-\chi^2)$) and the maximum probability corresponds to the best-fit parameters for this source. The 1σ uncertainty of each parameter can be derived from the Gaussian fits to the profiles of its p distribution by setting other parameters at its best-fit values.

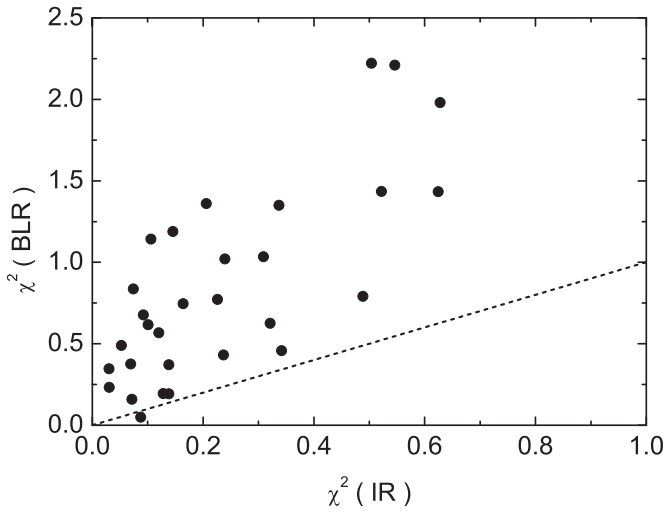

Figure 1. χ^2 values derived from multiwavelength SED fittings with the IR seed photons of the torus are plotted against the fittings with BLR seed photons. The dashed line represents $y = x$.

4. RESULTS

It is well known that the one-zone leptonic model cannot explain the low-frequency radio emission, which mainly originates from a large-scale jet. In this work, we consider data with $\log \nu \geqslant 11.5$ ($\nu \geqslant 300$ GHz or wavelength $\lambda \leqslant 1$ mm) in our SED modelings where the synchrotron radiation roughly becomes transparent in our model for the typical jet parameters of LSP blazars. The putative UV excess (big blue bump) of four sources (J1911−2006, J2148+0657, J2203+3145 and J2232+1143) was not included in the modeling, which is thought to be produced by the standard cold accretion disk (Shakura & Sunyaev 1973). We find that these four sources tightly follow the relation between optical luminosity and broad emission line luminosity defined by radio quiet AGNs, while most other LSP blazars have much brighter optical emission at a given emission-line luminosity, which supports the idea that the optical emission of these four sources indeed come primarily from the accretion disk as in RQ AGNs while that of other sources mainly comes from the jet (e.g., see Figures 3 and 4 in Liu & Jiang 2006, and references therein). In Figures 9–14, we show the best-fit SEDs of LSP blazars with seed photons from the molecular torus (left panel) and BLR (right panel), respectively. The dotted, dot-dashed, dashed, and solid lines represent the synchrotron, SSC, EC, and total emission, respectively. We find that the fittings with IR seed photons are systematically better than the BLR fitting based on their χ^2 values (see Figure 1), where these χ^2 values are shown in Columns 13 and 14 of Table 1, respectively. There is only one source (J2007−4434) for which the fitting with seed photons from BLR is better than that from the IR torus, but the χ^2 values of these two cases are still more or less similar. Therefore, our results suggest that the seed photons from the molecular torus for IC should be better than that from the BLR in most of the bright LSP blazars. We list the best-fit values of the parameters and their 1σ errors for the modeling with IR seed photons in Table 1. For example, Figure 2 shows the probability distribution of each parameter for J0522−3627, where $B = 0.93 \pm 0.04$ G, $\delta = 9.67 \pm 0.19$, $\gamma_{\rm min} = 47.54 \pm 13.73$, $\gamma_{\rm b} = (1.59 \pm 0.11) \times 10^3$, $p_1 = 2.35 \pm 0.01$, $p_2 = 4.51 \pm 0.12$, and $N_0 = (2.11 \pm 0.12) \times 10^5$. In the following analysis, we will

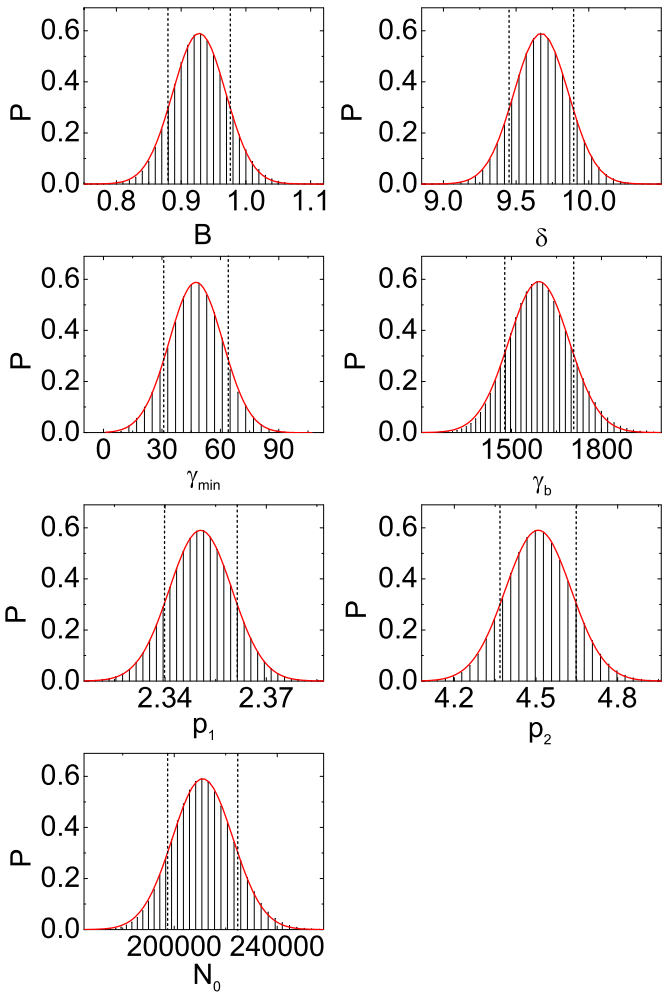

Figure 2. Example (J0522−3267) of a probability distribution for each parameter in the SED modeling along with the Gaussian fits (solid lines) where the vertical dashed lines correspond to a 1σ range of parameters.

(A color version of this figure is available in the online journal.)

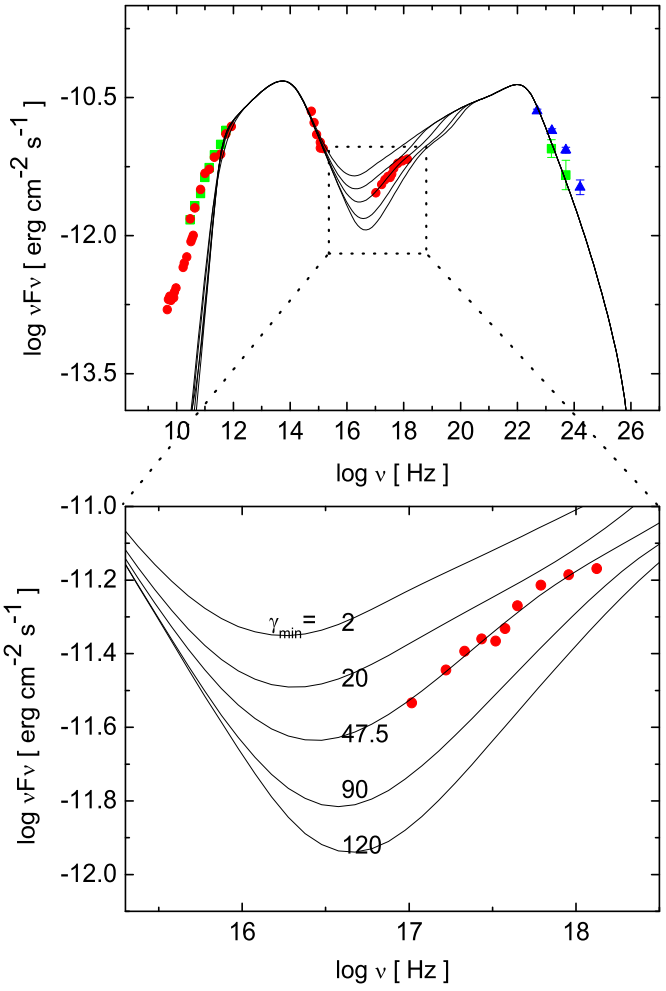

Figure 3. SED of models with different $\gamma_{\rm min}$ values for J0522−3267. The solid lines from top to bottom represent $\gamma_{\rm min}$ = 2, 20, 47.5 (the best-fit value), 90, and 120, respectively.

(A color version of this figure is available in the online journal.)

mainly consider the fitting results with seed photons originating from the torus.

In Figure 3, we present the SEDs predicted by our model with different $\gamma_{\rm min}$ values for the case of J0522−3627. It can be found that the shape of the soft X-ray spectrum (e.g., 0.1–10 keV) is very sensitive to this parameter. Therefore, it is possible to constrain the parameter $\gamma_{\rm min}$ for the selected LSP blazars. Through the fitting, we find that $\gamma_{\rm min}$ of these LSP blazars range from 5 to 160, with a median value of 55, where its distribution is shown in the top panel of Figure 4. The $\gamma_{\rm min}$ value is roughly not affected by the possible external seed photons since the soft X-ray spectrum primarily originates from the SSC emission. We also show the distribution of $\gamma_{\rm min}$ which is constrained from the fittings with seed photons from BLR in the bottom panel of Figure 4. It can be seen that both distributions are more or less similar (top and bottom panels).

The jet power carried by relativistic electrons, protons, the magnetic field, and radiation can be calculated from the parameters in our SED fittings (e.g., Celotti et al. 1993; Celotti & Ghisellini 2008) through

$$P_i = \pi R^2 \Gamma^2 c U_i', \quad (2)$$

where U_i' is the energy density of the i component as measured in the comoving frame, which is given by

$$U_e' = m_e c^2 \int N(\gamma)\gamma d\gamma, \quad (3)$$

$$U_p' = m_p c^2 \int N(\gamma) d\gamma, \quad (4)$$

$$U_B' = B^2/8\pi, \quad (5)$$

$$U_r' = \frac{L_{\rm obs}}{4\pi R^2 c \delta^4} \simeq \frac{L}{4\pi R^2 c \delta^4}, \quad (6)$$

where $L_{\rm obs}$ is the total observed non-thermal luminosity and L is the nonthermal luminosity derived from the modeling. Here we assume that there is one cold proton per emitting electron ($n_p = n_e$). The powers carried by each component, P_p, P_e, P_B, and P_r are reported in Table 2.

In Figure 5, we present the relation between the power in the bulk motion of electrons, protons, and the magnetic field ($P_{\rm jet} = P_e + P_p + P_B$) and the 151 MHz radio luminosity L_{151} for the LSP blazars, where the 151 MHz radio fluxes are selected from NED[4] (see Table 2). For comparison, we also present the

[4] http://ned.ipac.caltech.edu/forms/byname.html

Table 2
Jet Power

J2000.0 Name	F_{151}[a] (Jy)	$P_{\rm jet}^{151}$ (erg s^{-1})	$P_{\rm jet}$[b] (erg s^{-1})	P_B (erg s^{-1})	P_e (erg s^{-1})	P_p (erg s^{-1})	P_r (erg s^{-1})	$P_p^{'}$[c] (erg s^{-1})	η
(1)	(2)	(3)	(4)	(4)	(6)	(7)	(8)	(9)	(10)
J0136+4751	1.47	45.51	46.83 ± 0.30	46.20 ± 0.20	44.98 ± 0.28	46.71 ± 0.32	44.92 ± 0.06	...	0
J0237+2848	2.33	45.80	46.77 ± 0.18	46.18 ± 0.14	44.85 ± 0.16	46.63 ± 0.19	44.98 ± 0.03	...	0
J0334−4008	2.10	45.95	46.25 ± 0.32	45.67 ± 0.20	45.12 ± 0.32	46.07 ± 0.36	45.39 ± 0.07	45.23 ± 0.54	0.13 ± 0.04
J0457−2324	2.83	45.78	46.90 ± 0.55	45.27 ± 0.18	45.30 ± 0.50	46.88 ± 0.56	45.12 ± 0.04	45.42 ± 0.60	0.07 ± 0.03
J0522−3627	76.72	44.87	45.15 ± 0.10	43.54 ± 0.05	43.99 ± 0.09	45.11 ± 0.11	43.08 ± 0.02	44.81 ± 0.11	0.67 ± 0.01
J0538−4405	3.67	45.82	46.45 ± 0.22	46.22 ± 0.18	44.96 ± 0.23	46.03 ± 0.26	45.30 ± 0.06	...	0
J0854+2006	7.10	45.23	45.43 ± 0.23	44.92 ± 0.15	44.27 ± 0.23	45.22 ± 0.26	44.19 ± 0.04	44.80 ± 0.31	0.55 ± 0.22
J1058−0133	5.56	45.85	46.26 ± 0.18	45.59 ± 0.09	45.00 ± 0.17	46.12 ± 0.20	44.97 ± 0.03	45.30 ± 0.29	0.27 ± 0.11
J1130−1449	4.04	45.97	46.23 ± 0.15	45.78 ± 0.10	45.07 ± 0.15	45.99 ± 0.17	45.25 ± 0.03	45.10 ± 0.37	0.12 ± 0.02
J1159+2914	4.28	45.63	45.95 ± 0.31	45.19 ± 0.20	44.77 ± 0.30	45.83 ± 0.34	44.66 ± 0.05	45.31 ± 0.39	0.46 ± 0.17
J1222+0413	2.47	45.72	45.99 ± 0.11	45.64 ± 0.10	44.92 ± 0.10	45.66 ± 0.11	45.09 ± 0.03	...	0
J1229+0203	97.95	45.63	46.13 ± 0.14	44.30 ± 0.10	44.98 ± 0.12	46.09 ± 0.14	44.85 ± 0.03	45.49 ± 0.15	0.40 ± 0.01
J1256−0547	22.08	45.99	46.23 ± 0.16	45.51 ± 0.09	45.17 ± 0.15	46.09 ± 0.17	45.41 ± 0.03	45.56 ± 0.21	0.45 ± 0.08
J1505+0326	2.49	45.08	45.38 ± 0.21	44.06 ± 0.10	44.26 ± 0.19	45.32 ± 0.22	43.81 ± 0.03	44.98 ± 0.22	0.63 ± 0.03
J1517−2422	2.20	43.90	44.76 ± 0.20	43.35 ± 0.15	43.92 ± 0.18	44.67 ± 0.21	43.38 ± 0.01	43.45 ± 0.28	0.11 ± 0.04
J1642+3948	12.39	45.82	46.77 ± 0.39	45.26 ± 0.14	45.22 ± 0.35	46.74 ± 0.40	44.94 ± 0.05	45.58 ± 0.43	0.13 ± 0.03
J1800+7828	2.09	45.47	45.92 ± 0.19	45.46 ± 0.13	44.75 ± 0.19	45.69 ± 0.22	44.91 ± 0.04	...	0
J1833−2103	10.74	46.74	47.90 ± 0.25	45.80 ± 0.27	45.87 ± 0.21	47.90 ± 0.25	46.00 ± 0.06	46.57 ± 0.28	0.09 ± 0.01
J1911−2006	2.70	45.91	47.12 ± 0.15	45.40 ± 0.14	45.55 ± 0.12	47.10 ± 0.15	45.45 ± 0.02	45.42 ± 0.24	0.04 ± 0.01
J1923−2104	2.73	45.70	46.12 ± 0.15	45.69 ± 0.11	44.88 ± 0.14	45.89 ± 0.16	45.13 ± 0.03	...	0
J2007−4434	1.52	43.83	45.26 ± 0.14	43.54 ± 0.08	44.15 ± 0.12	45.22 ± 0.14	43.40 ± 0.03	42.79 ± 0.38	0.01 ± 0.01
J2148+0657	3.50	45.80	47.22 ± 0.16	45.28 ± 0.14	45.53 ± 0.13	47.21 ± 0.16	45.01 ± 0.04	45.50 ± 0.22	0.04 ± 0.01
J2151−3027	1.89	46.31	46.39 ± 0.08	45.51 ± 0.07	45.56 ± 0.06	46.25 ± 0.08	45.89 ± 0.02	45.89 ± 0.09	0.61 ± 0.04
J2202+4216	1.77	44.03	45.92 ± 0.52	43.78 ± 0.09	44.26 ± 0.47	45.90 ± 0.52	43.49 ± 0.03	43.06 ± 0.66	0.003 ± 0.002
J2203+3145	3.50	45.01	46.98 ± 0.21	44.56 ± 0.13	44.98 ± 0.18	46.97 ± 0.21	44.02 ± 0.03	44.69 ± 0.28	0.01 ± 0.003
J2207−5346	5.65	46.02	46.01 ± 0.20	45.78 ± 0.16	44.73 ± 0.22	45.56 ± 0.25	44.95 ± 0.05	45.50 ± 0.27	0.94 ± 0.39
J2229−0832	2.72	46.05	46.34 ± 0.19	45.98 ± 0.14	45.15 ± 0.19	46.05 ± 0.22	45.42 ± 0.04	...	0
J2232+1143	5.66	45.93	46.06 ± 0.21	45.31 ± 0.18	44.96 ± 0.19	45.93 ± 0.22	44.87 ± 0.04	45.71 ± 0.23	0.75 ± 0.11
J2253+1608	14.03	46.50	46.92 ± 0.25	46.33 ± 0.20	45.79 ± 0.22	46.75 ± 0.25	46.32 ± 0.05	...	0
J2327+0940	1.41	46.02	46.27 ± 0.16	45.87 ± 0.13	45.20 ± 0.15	45.98 ± 0.18	45.53 ± 0.04	...	0

Notes.
[a] F_{151} is the flux in 151 MHz, which is selected from NED.
[b] $P_{\rm jet} = P_p + P_e + P_B$ is the jet power in the bulk motion of protons, electrons, and the magnetic field.
[c] $P_p^{'}$ is the jet power carried by a proton after considering a fraction of $e^{\pm}$ pairs in the jet.

$P_{\rm jet} - L_{151}$ relation for a sample of FR I (empty stars) and FR II (empty squares) radio galaxies (see Godfrey & Shabala 2013, for more details), where the jet kinetic power of FR Is and FR IIs are estimated from the X-ray cavities and cocoon dynamics respectively. We can clearly see that the jet kinetic power of blazars is systematically higher than that of FR I/IIs at the given 151 MHz radio luminosity, even though FR IIs are normally regarded as the same as LSP blazars in the unification scheme except for their jet viewing angles. We speculate that it may be caused by assuming that there is one proton per emitting electron in the jet and that the jet power will be reduced if the jet also includes a fraction of $e^{\pm}$ pairs.

To evaluate the possible positrons in the jet, we further assume $n_p = \eta n_{e^-}$ and $n_{e^+} = (1-\eta) n_{e^-}$ in the model, where $\eta = 1$ corresponds to a normal jet with pure e^-–p plasma while $\eta = 0$ corresponds to a jet with pure $e^{\pm}$ pairs. In this case, the number density of protons and the jet power carried by protons will be reduced by a factor of $\eta/(2-\eta)$ since positrons emit with the same kind of energy spectrum as electrons. It is possible to derive the value of η if the jet power is known from an independent method. To do this, we calculate the jet kinetic power of these LSP blazars from their 151 MHz radio luminosities using the relation of $P_{\rm jet}$–L_{151} for FR IIs (Godfrey & Shabala 2013),

$$P_{\rm jet}^{151} = 3 \pm 1 \times 10^{44} \left(\frac{L_{151}}{10^{25}\ {\rm W\ Hz^{-1}\ sr^{-1}}} \right)^{0.67 \pm 0.05}, \quad (7)$$

where the jet kinetic power of FR IIs is estimated from their cocoon dynamics. $P_{\rm jet}^{151}$ derived from Equation (7) for each LSP blazar is listed in Table 2. By setting $P_{\rm jet} = P_{\rm jet}^{151}$, we derive the η values for 21 sources, which are listed in Column 10 of Table 2. We noted that the other nine sources have $P_B + P_e \gtrsim P_{\rm jet}^{151}$, which may be caused by the uncertainties in jet power estimation from $P_{\rm jet} - L_{151}$ or by the uncertainties in the SED modeling. The jet power carried by protons is most possibly negligible in these nine blazars and we will simply assume $\eta \simeq 0$ in them. The distribution of η is shown in Figure 6 where the median η value is 0.08 (average η value is 0.22). The jet power for cold protons, $P_p^{'}$, electrons/positrons, P_e, Poynting flux, P_B, and radiation, P_r, were presented in Figure 7 when considering the possible $e^{\pm}$ pairs, where the total jet power estimated from L_{151} is also shown in the bottom panel (dashed lines represent median values).

In Figure 8, we compare the Doppler factor, δ, which is derived from our SED fittings with the variability Doppler

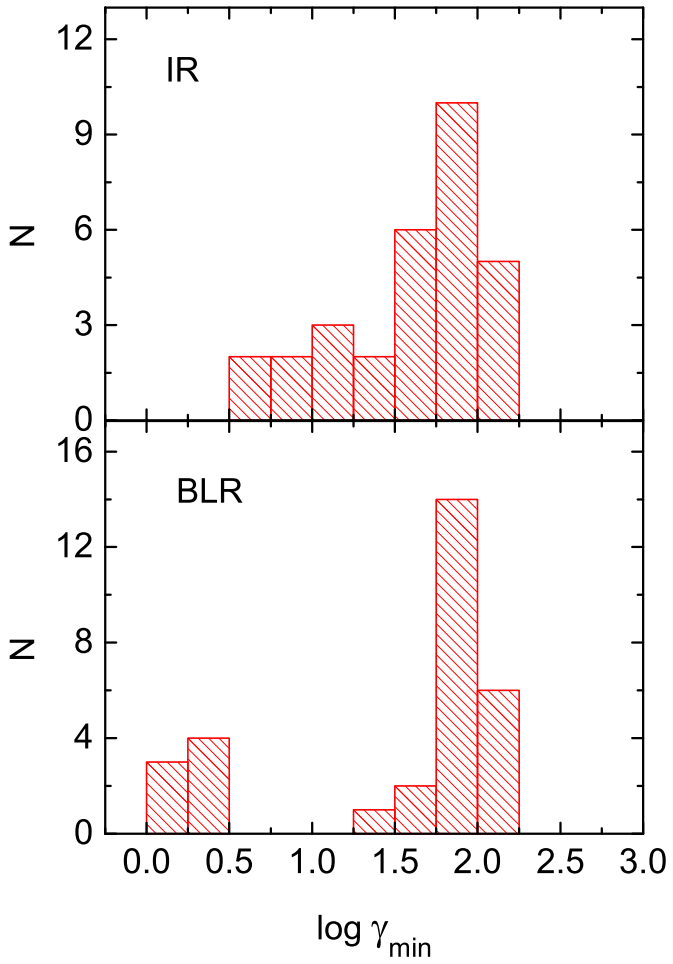

Figure 4. Distribution of the parameter $\gamma_{\rm min}$ for our sample, where the top and bottom panels represent fittings with seed photons from the IR torus and BLR, respectively.

(A color version of this figure is available in the online journal.)

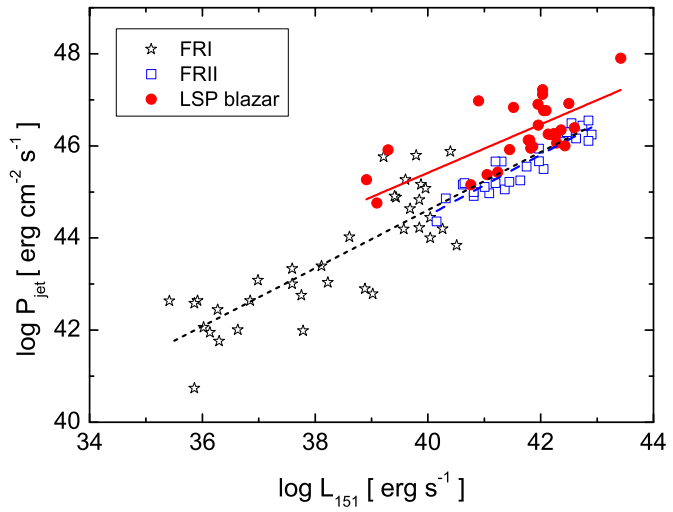

Figure 5. Relation between the jet kinetic power, $P_{\rm jet}$, and 151 MHz radio luminosity, L_{151}. The solid points represent the LSP blazars where the jet kinetic power is derived from the parameters in the SED fitting assuming one proton per emitting electron in the jet. For comparison, the empty stars and squares represent the FR I/IIs where the jet power is estimated from X-ray cavities (FR Is) and cocoon dynamics (FR IIs), respectively. The solid, dashed, and dotted lines represent the best fits for LSP blazars, FR IIs, and FR Is/IIs, respectively.

(A color version of this figure is available in the online journal.)

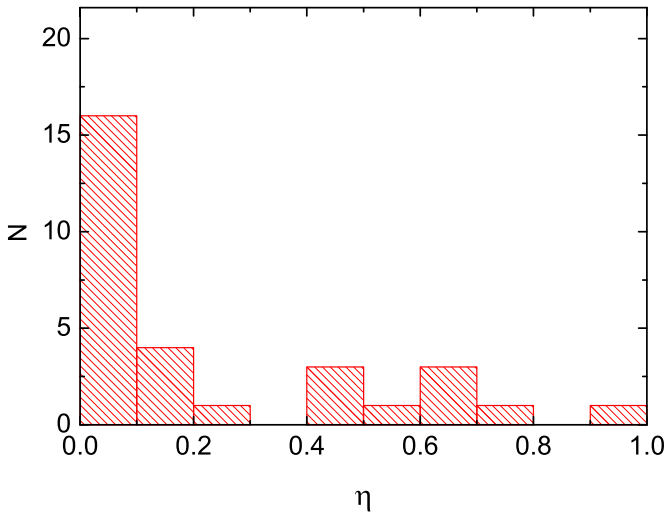

Figure 6. Distribution for the η values, where $\eta = n_p/n_{e^-}$.

(A color version of this figure is available in the online journal.)

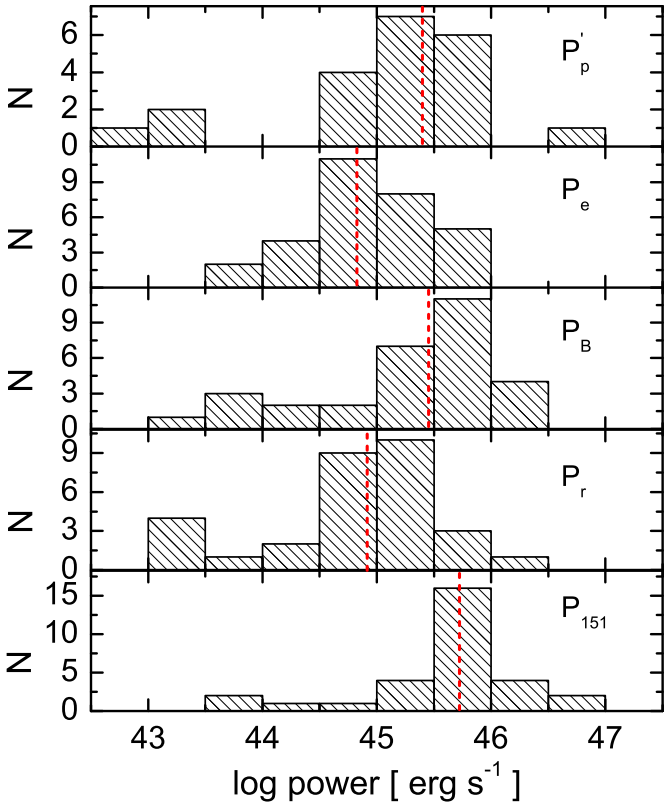

Figure 7. Distributions of jet power carried by cold protons ($P_p^{'}$), positrons/electrons (P_e), Poynting flux (P_B), radiation (P_r), and total power derived from $L_{151\,\rm MHz}$ (from top to bottom panels), where we have assumed the jet includes a fraction of $e^{\pm}$ pairs. The dashed line in each panel shows the median value.

(A color version of this figure is available in the online journal.)

factor, $\delta_{\rm var}$, which is estimated from the variability brightness temperature by assuming the intrinsic brightness temperature is limited to an equipartition value (Savolainen et al. 2010, see also Hovatta et al. 2009; Fan et al. 2009 for more details). They are positively correlated (Pearson correlation coefficient $r = 0.71$ and chance probability $p < 1\%$) and roughly consistent with each other.

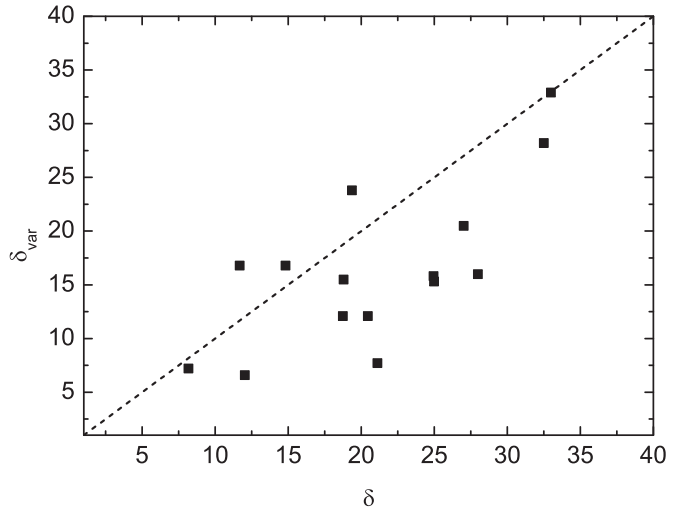

Figure 8. Doppler factor derived from SED fitting vs. that derived from radio variability, where the dashed line represents $y = x$.

5. DISCUSSION AND CONCLUSION

5.1. Modeling the Overall SEDs

The simultaneous or quasi-simultaneous *Plank*, *Swift*, *Fermi*, and ground-based observations for a sample of blazars provide a great opportunity to explore their jet properties through modeling their SEDs. Our model roughly becomes transparent at the submillimeter waveband for the typical jet parameter of LSP blazars. The fairly good correlation of the variability between millimeter and optical signals (e.g., Sikora et al. 2008) or between γ-ray and millimeter signals (e.g., Wehrle et al. 2012; D'Ammando et al. 2013; Orienti et al. 2013) also supports this scenario. Therefore, the emission from millimeter to γ-rays may originate from a more or less similar region (León-Tavares et al. 2012), and it should be reasonable to fit these data with the one-zone homogeneous model. From the fitting results, we find that the first hump from the millimeter to the optical band can be well reproduced by the synchrotron emission, while the second hump can be reproduced by SSC and EC emission for these LSP blazars (see Figures 9–14). Note that the 1σ uncertainty of the model parameter in Table 1 is derived by setting other parameters to their best-fit values, which may be underestimated if we allow all the parameters to be free (particularly in the case of the possible degeneracy in the model). The observational data are not very good in a few sources (e.g., only eight points in J1911−2006, or data is absent in a certain waveband), which will not affect our main conclusion in a statistical sense. The consistency of the Doppler factor from the SED fitting with that derived from an independent method suggest that our SED modeling should be reasonable, even though there is no reason why the radio Doppler factor should be the same as that derived from the γ-ray emitting region (e.g., Fan et al. 2013).

5.2. Seed Photon Field and Location of γ-Ray Emitting Region

For LSP blazars, the γ-ray emission is mainly contributed by the EC process, and two main candidates of external seed fields have been proposed. The first one is the BLR if the γ-ray emitting region stays inside the BLR, which can easily explain the short variability timescales reported in some γ-ray observations of blazars (e.g., Ackermann et al. 2010; Foschini et al. 2011), even though these timescales do not necessarily imply a short distance to the BH. The second candidate is the molecular torus if the γ-ray emitting region stays outside the BLR and is up to $\sim 10^5 R_S$ (e.g., Jorstad et al. 2010; Agudo et al. 2011). In this work, we explore this issue through the SED modelings, where external seed photons from either the BLR or the molecular torus are considered. Based on χ^2 tests, we find that the soft photons may come predominantly from the IR torus in these LSP blazars (see Figure 1), which may be caused by the KN effect. Assuming a typical seed photon frequency $\nu_{\rm ext}$, Compton scattering by the electron with a Lorentz factor γ yields $\nu_{\rm EC}^{\rm T} \approx (4/3)\nu_{\rm ext}\gamma^2\Gamma^2$ within the Thomson regime in the observational frame (assuming $\delta \approx \Gamma$). Combining the Thomson scattering condition $4\gamma h\nu_{\rm ext}\Gamma/m_e c^2 \lesssim 1$, we obtain $\nu_{\rm EC}^{\rm T} \lesssim (1/12)(m_e c^2)^2/(h^2\nu_{\rm ext})$. If seed photons come from the BLR, we get $\nu_{\rm EC,BLR}^{T} \lesssim 6\times 10^{23}$ Hz for $\nu_{\rm ext,BLR} \approx 2\times 10^{15}$ Hz (see also Cao & Wang 2013). This implies that the IC emission would be significantly suppressed by the KN effect if $\nu \gtrsim 6\times 10^{23}$ Hz, which will lead to a very steep spectrum. However, we have $\nu_{\rm EC,torus}^{T} \lesssim 4\times 10^{25}$ Hz $\sim$ 165 GeV if the main seed photons come from the dust torus with $\nu_{\rm ext,torus} \approx 3\times 10^{13}$ Hz. Therefore, the γ-ray spectrum of the EC model with IR seed photons will not become very steep spectrum at observational band. This can roughly explain why the fittings are systematically better for the EC model with IR seed photons (see also Liu & Bai 2006; Cao & Wang 2013). Chen & Bai (2011) proposed that the IR external field may play an important role through analyzing the ratio of EC to synchrotron luminosity for a sample of *Fermi* bright blazars. Sikora et al. (2009) found that the bright blazars favor seed photons from the molecular torus over those from the BLR based on the lack of bulk-Compton and KN features in the broadband spectra.

Our modeling results provide indirect evidence that the γ-ray emitting region may be located outside the BLR and within the molecular torus, which roughly corresponds to several thousand to $10^5 R_S$ from the BH. We note that the location of the γ-ray emitting region should be determined by the energy dissipation or particle acceleration processes within the relativistic jet that are responsible for the generation of nonthermal electrons. Asada et al. (2014) explored the velocity field of the M87 jet and found that the jet matter is mainly accelerated in a region of $\sim 10^5 R_S$, and the jet is decelerated at larger radii. Asada et al.'s (2014) result suggests that most of the jet energy was dissipated at $\sim 10^5 R_S$, which may correspond to the γ-ray emitting region of LSP blazars (e.g., $R_{\rm diss} > R_{\rm BLR}$). The detection of γ-rays with a rest-frame energy above 20 GeV (e.g., Aleksi et al. 2011; Pacciani et al. 2012) suggests that the γ-ray emitting region should be located outside the highly opaque ($\tau \approx$ 5–10) BLR, which would not permit photons of such high energies to escape (e.g., Donea & Protheroe 2003; Bai et al. 2009; Poutanen & Stern 2010; Brown 2013; Tavecchio et al. 2013). Based on the simultaneous flares at millimeter and γ-ray wavebands, it was also suggested that the γ-ray emitting region should be far away from the BLR region where the high-energy photons should be produced in a region that is already transparent to the radiation at millimeter wavelengths (e.g., Jorstad et al. 2010; Marscher et al. 2010; Agudo et al. 2011; León-Tavares et al. 2011; D'Ammando et al. 2013; Orienti et al. 2013). Through the correlation of the millimeter with γ-ray light curves and direct ultrahigh-resolution 7 mm imaging with the Very Long Baseline Array, Agudo et al. (2011) argued that the location of the γ-ray emitting region should be >14 pc from the BH in the jet of OJ 287, which roughly corresponds to $\gtrsim 10^4 R_S$ if we consider the BH mass to be $\sim 10^{10} M_\odot$ (e.g., Valtonen et al. 2012). This independent evidence supports our

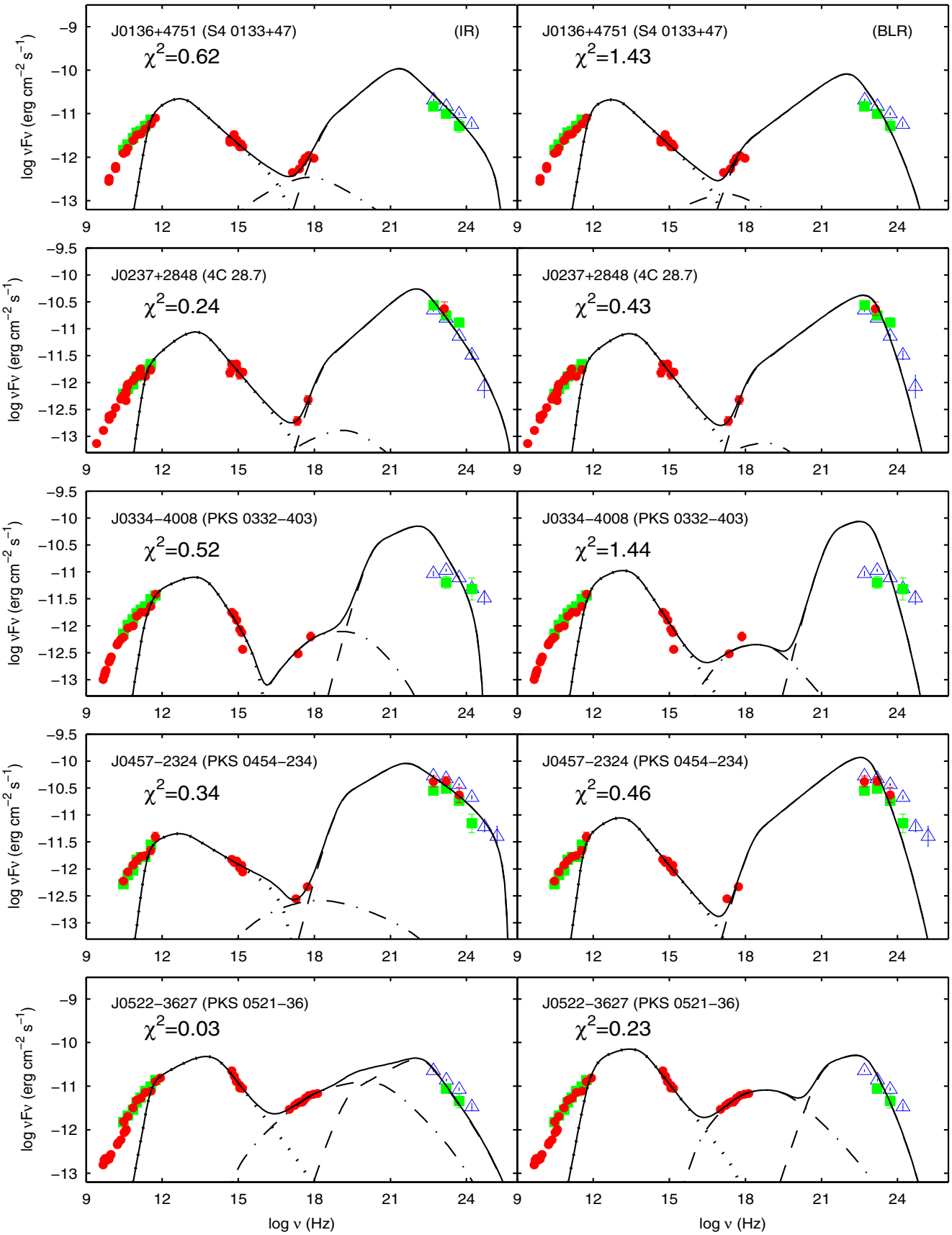

Figure 9. SEDs of J0136+4751, J0237+2848, J0334−4008, J0457−2324, and J0522−3627, together with the fittings, where the model parameters are listed in Table 1. The red circles represent the simultaneous data, the green squares represent the quasi-simultaneous data, and the blue triangles represent *Fermi* data integrated over 27 months. The left and right panels represent the fittings with seed photons from the IR molecular torus and the BLR, respectively, in the EC process. The dotted, dot-dashed, and dashed lines represent the synchrotron, SSC, and EC emission, respectively.

(A color version of this figure is available in the online journal.)

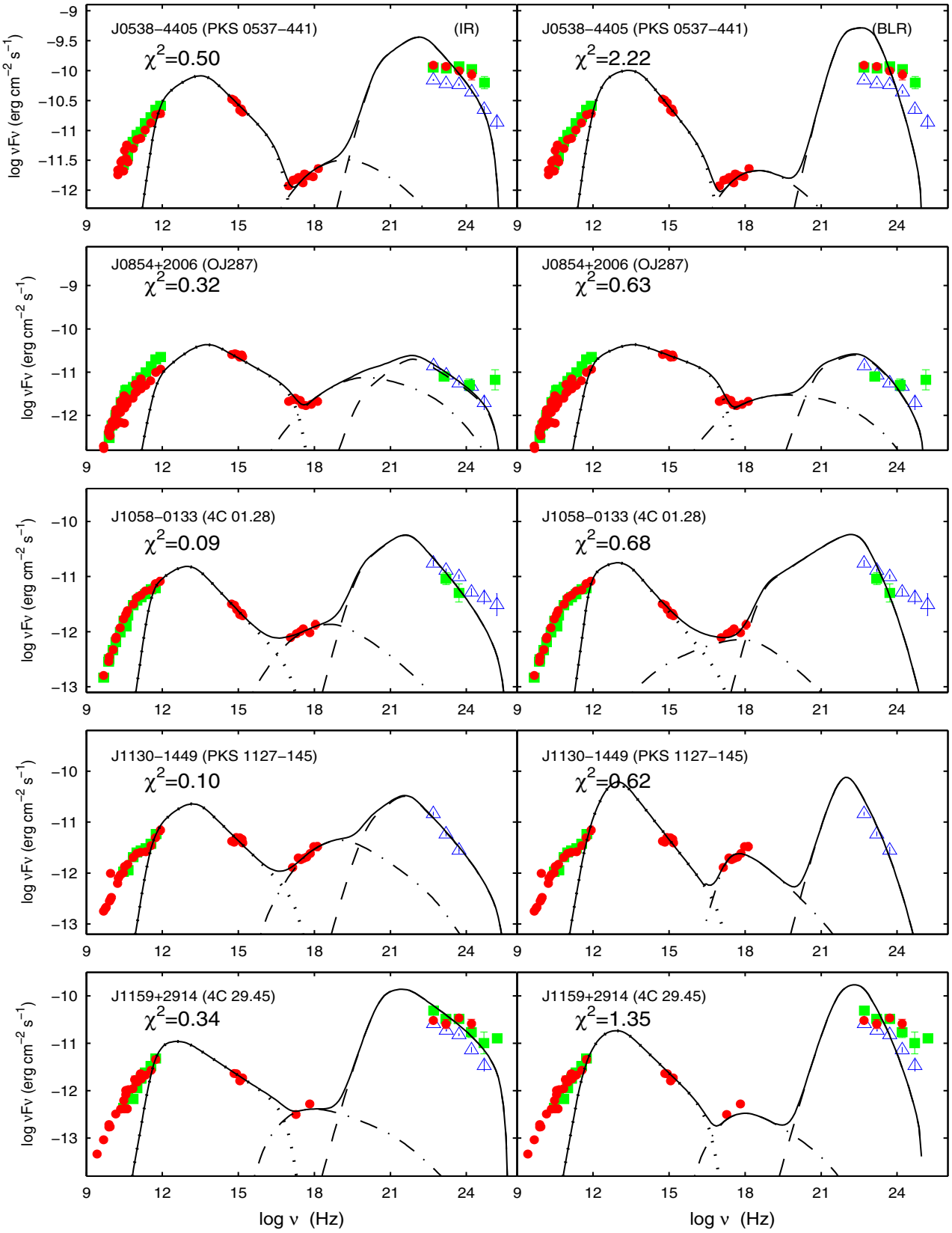

Figure 10. SEDs of J0538−4405, J0854+2006, J1058−0133, J1130−1449, and J1159+2914. Symbols and lines are as in Figure 9.
(A color version of this figure is available in the online journal.)

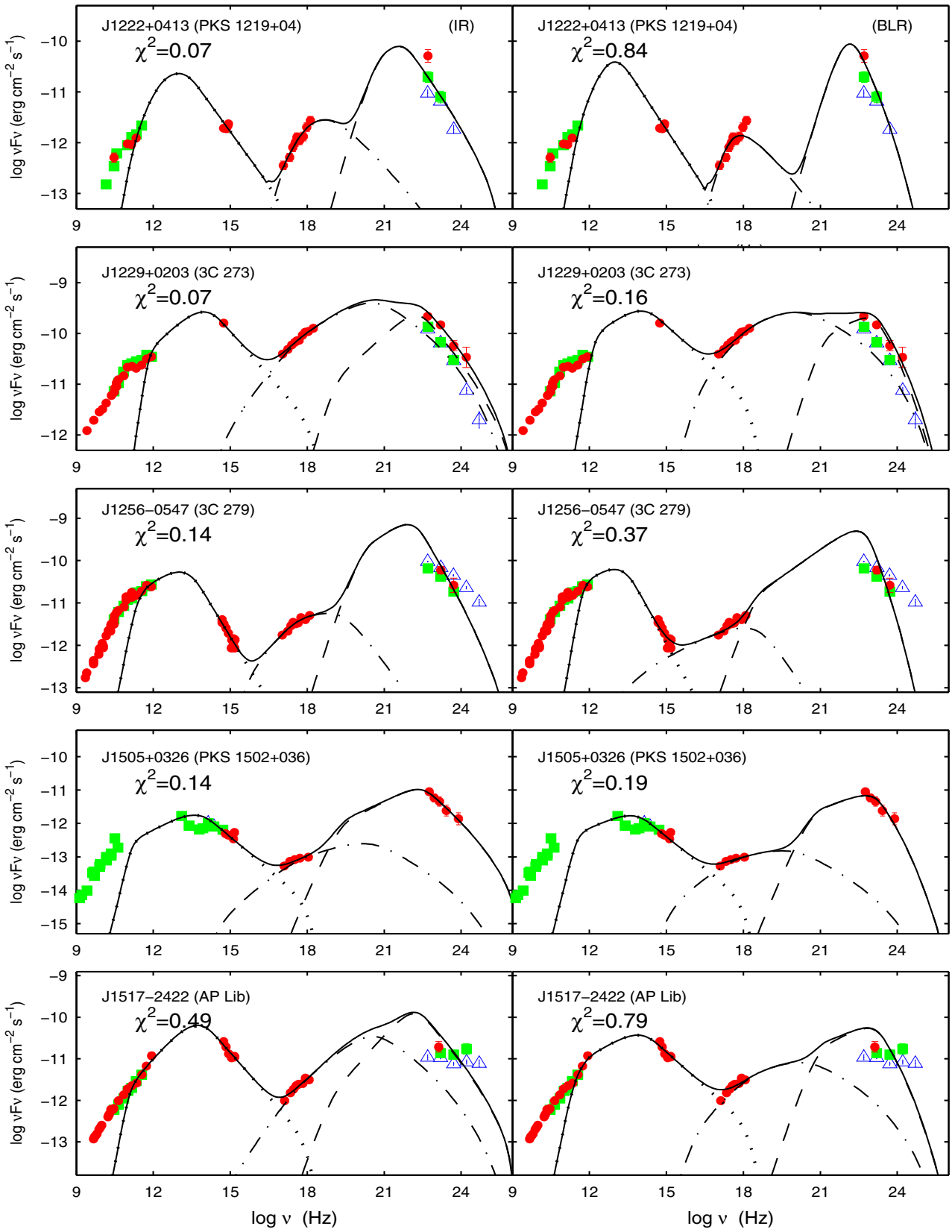

Figure 11. SEDs of J1222+0413, J1229+0203, J1256−0547, J1505+0326, and J1517−2422. Symbols and lines are as in Figure 9.
(A color version of this figure is available in the online journal.)

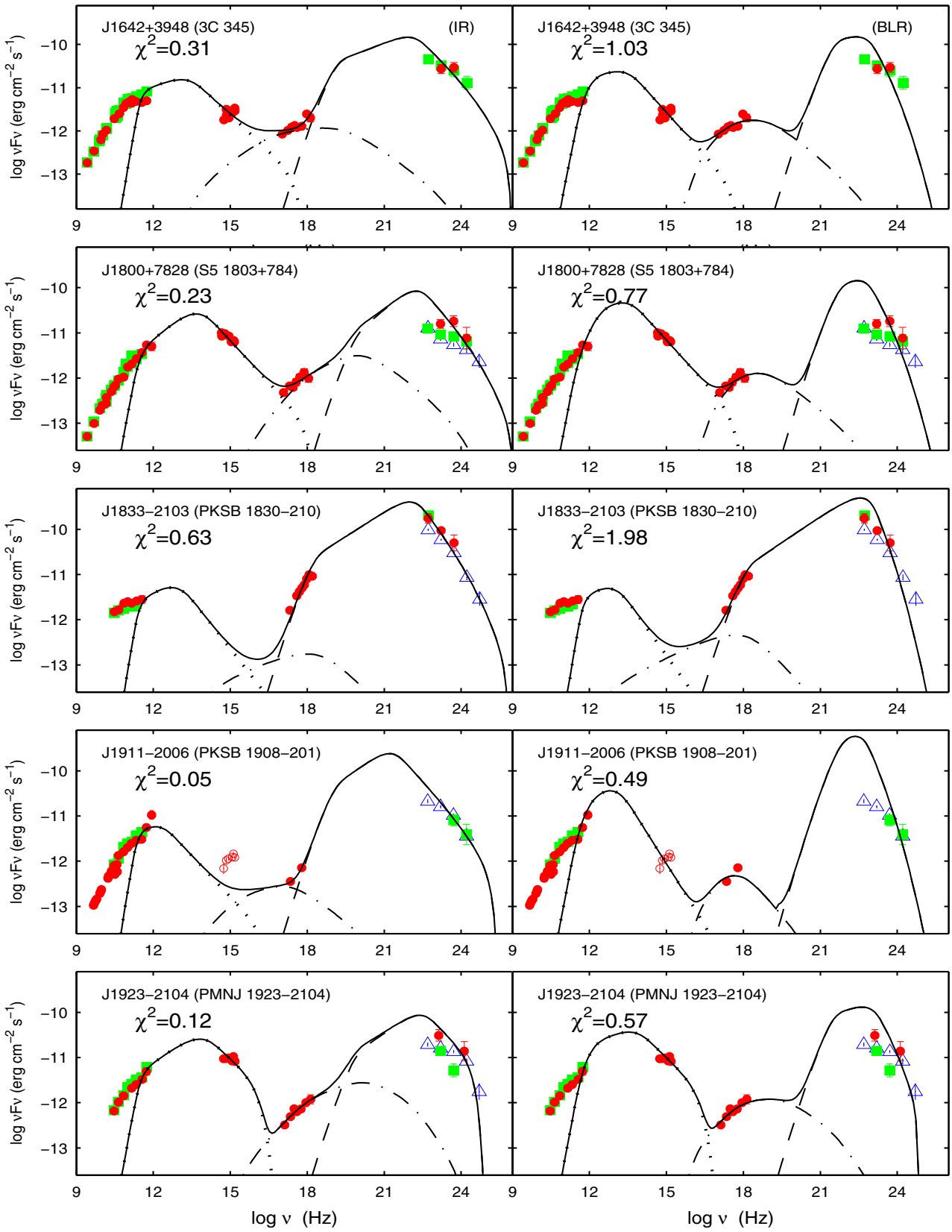

Figure 12. SEDs of J1642+3948, J1800+7828, J1833−2103, J1911−2006, and J1923−2104. Symbols and lines are as in Figure 9. The red open circles of J1911−2006, which may originate in the cold accretion disk, are not included in our modeling.

(A color version of this figure is available in the online journal.)

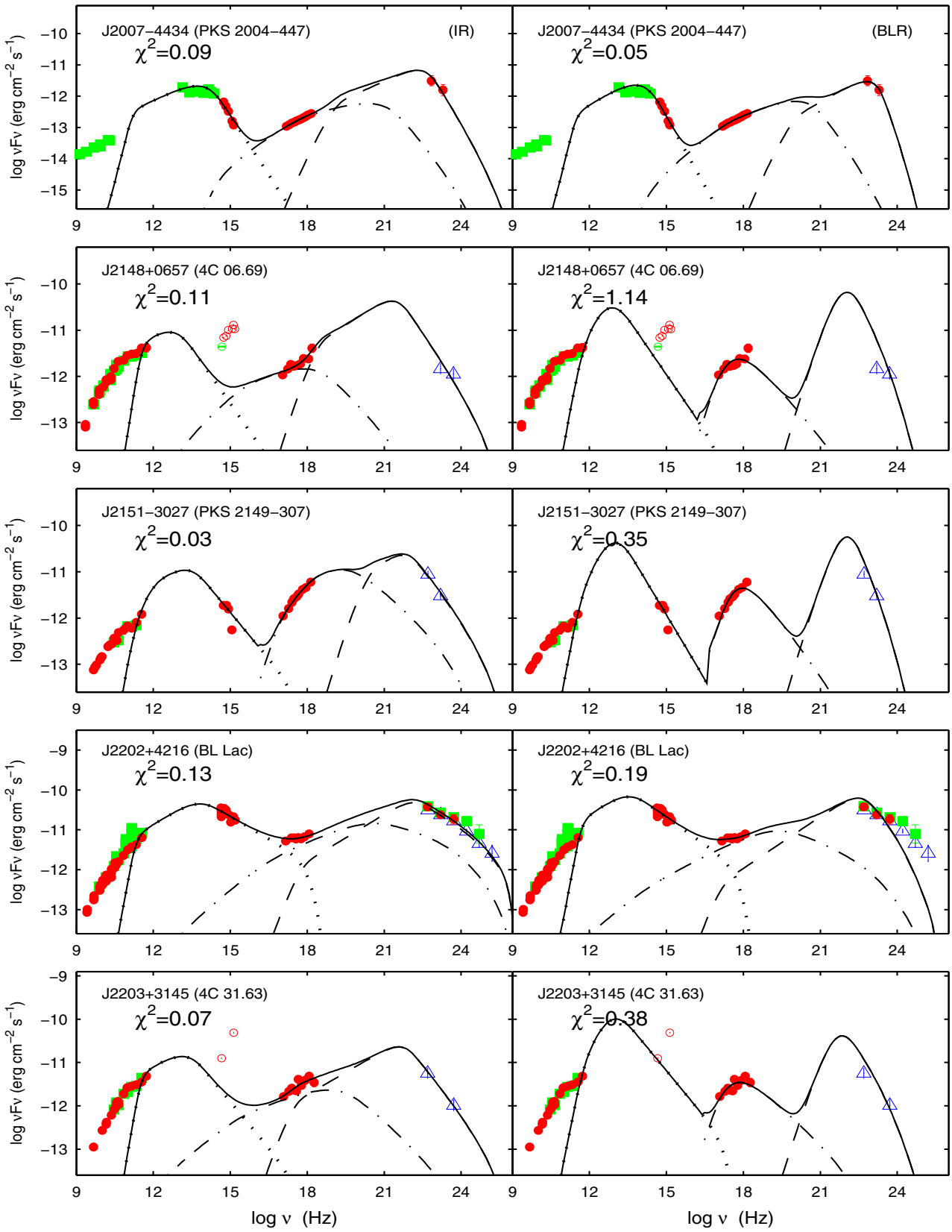

Figure 13. SEDs of J2007−4434, J2148+0657, J2151−3027, J2202+4216, and J2203+3145. Symbols and lines are as in Figure 9. The red open circles of J2148+0657 and J2203+3145, which may originate in the cold accretion disk, are not included in our modeling.

(A color version of this figure is available in the online journal.)

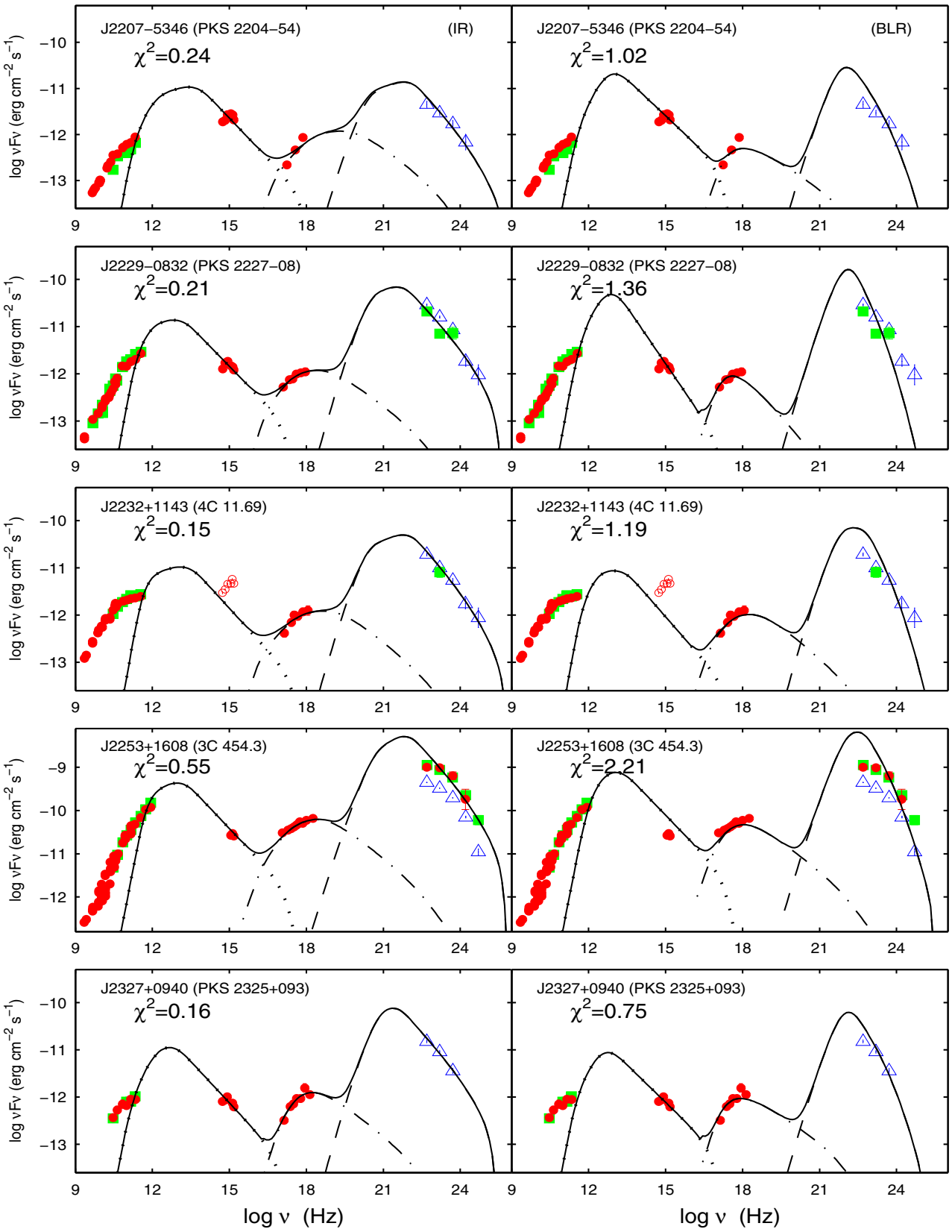

Figure 14. SEDs of J2207−5346, J2229−0832, J2232+1143, J2253+1608, and J2327+0940. Symbols and lines are as in Figure 9. The red open circles of J2232+1143, which may originate in the cold accretion disk, are not included in our modeling.

(A color version of this figure is available in the online journal.)

conclusions that the γ-ray emitting region may stay outside the BLR (several thousands of R_S) and the dominant seed photons for EC should be dominated by the dusty torus rather than the BLR.

5.3. γ_{min} Limits, Jet Power, and Jet Composition

It is well known that the minimum electron Lorentz factor (or the low-energy cutoff), $\gamma_{\rm min}$, plays a crucial role in estimating the powers in particles (e.g., $P_{\rm jet} \propto \gamma_{\rm min}^{1-p_1}$). Normally, this parameter is poorly constrained due to its synchrotron radiation being self-absorbed. However, these low-energy electrons would instead contribute to the low-energy part of SSC emission. The X-ray emission of LSP blazars is known to be dominated by SSC (i.e., Tavecchio et al. 2007; Celotti & Ghisellini 2008; Cao & Wang 2013; Zhang et al. 2014), which provides a possibility for constraining $\gamma_{\rm min}$ through modeling multiwavelength SEDs (see Figure 3). In this work, we select a sample of LSP blazars with good soft-X-ray data and find that $\gamma_{\rm min}$ ranges from 5 to 160 (with a median of 55) through SED modelings. It is interesting to note that the $\gamma_{\rm min}$ value is not sensitive to the possible external seed photon field because it was mainly constrained from the SSC process (see Figure 4). $\gamma_{\rm min}$ values around several tens for most of LSP blazars in our fittings are quite consistent with those reported in some recent works even though most of the fittings are evaluated by eye (e.g., Tavecchio et al. 2000; Chen et al. 2010; Paliya et al. 2013; Kushwaha et al. 2013; Dutka, et al. 2013; Potter & Cotter 2013). From a theoretical perspective, Sari et al. (1998) derived the minimum electron Lorentz factor $\gamma_{\rm min} = [(p-2)/(p-1)](m_p/m_e)\varepsilon_e\Delta\Gamma$ ($p \neq 2$) based on the electron energy distribution and jump conditions for a relativistic shock where ε_e is the fraction of shock energy that goes into the electrons, p is the index of the power-law electron distribution (e.g., $N_e \propto \gamma_e^{-p}$), and $\Delta\Gamma$ is the Lorentz factor difference for two colliding shells. We can derive $\gamma_{\rm min} \sim 40$ for a typical value of $p = 2.24$ for relativistic shock acceleration (e.g., Bednarz & Ostrowski 1998), $\varepsilon_e = 0.1$ in γ-ray bursts and blazars (e.g., Panaitescu & Kumar 2001; Wu et al. 2007) and $\Delta\Gamma \sim 1$ in blazars, which can roughly explain $\gamma_{\rm min} \sim$ several tens as constrained from the observations. It should be noted that the lower limits of $\gamma_{\rm min}$ are not well constrained for several sources (e.g., J0457−2324, J1517−2422, J1642+3948, J2202+4216, and J2203+3145), which is caused by poor observational data or both SSC and EC contributions to its X-ray emission.

With the constrained $\gamma_{\rm min}$, we calculate the jet power for each source. We find that the jet kinetic power of LSP blazars is systematically higher than that of FR IIs at given 151 MHz luminosity (see Figure 5) if assuming one proton per emitting electron in the jet, where these two types of AGNs are assumed to be intrinsically the same except for the jet viewing angle (e.g., Urry & Padovani 1995; Xu et al. 2009). One possible reason for this difference is that the jet includes some positrons, which will reduce the jet's power. The X-ray cavities/bubbles in galaxy clusters (or giant galaxies, i.e., Fabian et al. 2000; Bîrzan et al. 2004; Allen et al. 2006; Rafferty et al. 2006) and cocoons associated with FR I/II galaxies (i.e., Kino et al. 2012; Godfrey & Shabala 2013) provide a possibility for estimating the jet's power independently. Assuming the jet power of LSP blazars is intrinsically the same as that of FR IIs at a 151 MHz luminosity, we find that the jet of most of LSP blazars should be dominated by a pair plasma, where the median ratio of protons to electrons is around 0.08 or the number density of positrons is around 10 times higher than that of protons.

It should be noted that $P_{\rm jet} > P_{\rm jet}^{151}$ may also be caused by some fraction of kinetic jet power that is converted into radiation before it dissipates in hotspots on large scales. We find that the total radiative jet power normally occupies $\sim$ several percent of the jet kinetic power in these LSP blazars, where most of the jet radiation comes from the γ-ray emitting region. After subtracting the radiative power derived from our modeling (as an approximation for total radiative power), we find that the η value increases slightly with a median value of 0.22 (average value is 0.29). This means that the number density of positrons is still around four times higher than that of protons. The assumption of full nonthermal electrons in a jet may be too simple since only a small fraction of thermal electrons are accelerated into a power-law distribution and most electrons remain in the thermal pool. If this is the case, our conclusion will be strengthened since the radiation from these thermal electrons is much lower than that of nonthermal electrons but the jet kinetic power will increase and the η value will decrease (i.e., more positrons are needed). It should be noted that there are still large uncertainties in the estimation of jet power through the $P_{\rm jet} - L_{151\,\rm MHz}$ relation, and, therefore, our results should be only statistically meaningful. Based on the possible effect of the anisotropic external seed photon field in a jet comoving frame, Ghisellini & Tavecchio (2010) set an upper limit of $\sim$10–20 on the pair to proton number ratio (see also Kataoka et al. 2008). Sikora & Madejski (2000) claimed that the jets contain more $e^{\pm}$ pairs than protons based on the absence of bulk-Compton emission in FSRQs, but that jets are still dynamically dominated by protons. Based on the very long baseline interferometry observations and theory of SSA, it was also found that the jet should be dominated by $e^{\pm}$ plasma (e.g., Reynolds et al. 1996; Hirotani 2005; Dunn et al. 2006). Our conclusion is roughly consistent with these results even though they are derived from different methods.

5.4. Conclusion

In this work, we employ the one-zone homogeneous leptonic jet model and χ^2-minimization procedure to fit the simultaneous or quasi-simultaneous multi-waveband SEDs for a sample of LSP blazars where external seed photons originating from the IR torus and BLR are considered. Our main results are summarized below.

1. The SED fitting with external seed photons from the IR torus is systematically better than that with seed photons from the BLR. This result suggests that the γ-ray emitting region of these LSP blazars most possibly stays outside the BLR.
2. With the good quality soft X-ray data combined with other multi-wavelength observations, we find that the minimum electron Lorentz factors, $\gamma_{\rm min}$, range from 5 to 160 for these LSP blazars with a median value of 55, which is not affected by the possible uncertainties of external seed photons.
3. Assuming a one-to-one ratio of protons and electrons in a jet, we find that the jet power estimated from the fitting parameters is much higher than that of FR II galaxies at a 151 MHz radio luminosity even though they are assumed to be intrinsically the same in the unification scheme. Therefore, we propose a mixed composition of e^-–e^+–p in the jets of these LSP blazars. The number density of $e^{\pm}$ pairs should be several times higher than that of e^-–p pairs if we assume that the jet power of LSP blazars is the same as that of FR IIs at a 151 MHz radio luminosity.

We thank the anonymous referee for his/her helpful suggestions and comments which helped to clarify and improve our work. This work is supported by the NSFC (grants 11103003, 11133005, 11103060 and 11233006), the National Basic Research Program of China (2009CB824800), and the New Century Excellent Talents in University (NCET-13-0238).

REFERENCES

Abdo, A., Ackermann, M., Agudo, I., et al. 2010, ApJ, 716, 30
Abdo, A., Ackermann, M., Atwood, W. B., et al. 2009, ApJ, 697, 934
Ackermann, M., Ajello, M., Baldini, L., et al. 2010, ApJ, 721, 1383
Agudo, I., Marscher, A. P., Jorstad, S. G., et al. 2011, ApJ, 735, 10
Aleksi, C. J., Antonelli, L. A., Antoranz, P., et al. 2011, ApJL, 730, L8
Allen, S., Dunn, R., Fabian, A. C., Taylor, G. B., & Reynolds, C. S. 2006, MNRAS, 372, 21
Arbeiter, C., Pohl, M., & Schlickeiser, R. 2002, A&A, 386, 415
Asada, K., Nakamura, M., Doi, A., Nagai, H., & Inoue, M. 2014, ApJ, 781, 2
Bai, J. M., Liu, H. T., & Ma, L. 2009, ApJ, 699, 2002
Bednarz, J., & Ostrowski, M. 1998, PhRvL, 80, 3911
Bentz, M. C., Peterson, B. M., Netzer, H., et al. 2009, ApJ, 697, 160
Bîrzan, L., McNamara, B., Nulsen, P., Carilli, C., & Wise, M. 2008, ApJ, 686, 859
Bîrzan, L., Rafferty, D., McNamara, B., Wise, M., & Nulsen, P. 2004, ApJ, 607, 800
Blandford, R. D., & Znajek, R. L. 1977, MNRAS, 179, 433
Blazejowski, M., Sikora, M., Moderski, R., & Madejski, G. M. 2000, ApJ, 545, 107
Blumenthal, G. R., & Gould, R. J. 1970, RvMP, 42, 237
Böttcher, M., Basu, S., Joshi, M., et al. 2007, ApJ, 670, 968
Böttcher, M., & Chiang, J. 2002, ApJ, 581, 127
Brown, A. M. 2013, MNRAS, 431, 824
Cao, G., & Wang, J. C. 2013, MNRAS, 436, 2170
Cao, X. 2003, ApJ, 599, 147
Cao, X. 2010, ApJ, 724, 855
Cao, X. 2014, ApJ, 783, 51
Cao, X., & Spruit, H. C. 2013, ApJ, 765, 149
Cavagnolo, K. W., McNamara, B. R., Nulsen, P. E. J., et al. 2010, ApJ, 720, 1066
Celotti, A., & Fabian, A. C. 1993, MNRAS, 264, 228
Celotti, A., & Ghisellini, G. 2008, MNRAS, 385, 283
Chen, L., & Bai, J. M. 2011, ApJ, 735, 108
Chen, L., Bai, J. M., Zhang, J., & Liu, H. T. 2010, RAA, 10, 707
Cleary, K., Lawrence, C. R., Marshall, J. A., Hao, L., & Meier, D. 2007, ApJ, 660, 117
D'Ammando, F., Antolini, E., Tosti, G., et al. 2013, MNRAS, 431, 2481
Dermer, C. D., & Schlickeiser, R. 1993, ApJ, 416, 458
Donea, A.-C., & Protheroe, R. J. 2003, APh, 18, 377
Dutka, M. S., Ojha, R., Pottschmidt, K., et al. 2013, ApJ, 779, 174
Dunn, R. J. H., Fabian, A. C., & Celloti, A. 2006, MNRAS, 372, 1741
Elitzur, M., & Ho, L. C. 2009, ApJ, 701, 91
Fabian, A. C., Sanders, J. S., Ettori, S., et al. 2006, MNRAS, 318, 65
Fan, J.-H., Huang, Y., He, T.-M., et al. 2009, PASJ, 61, 639
Fan, J.-H., Yang, J.-H., Liu, Y., & Zhang, J.-Y. 2013, RAA, 13, 259
Fan, Z., Cao, X., & Gu, M. 2006, ApJ, 646, 8
Foschini, L., Ghisellini, G., Tavecchio, F., Bonnoli, G., & Stamerra, A. 2011, A&A, 530, 77
Fossati, G., Buckley, J. H., Bond, I. H., et al. 2008, ApJ, 677, 906
Ghisellini, G. 2012, MNRAS, 424, 26
Ghisellini, G., & Celotti, A. 2001, A&A, 379, 1
Ghisellini, G., Celotti, A., Fossati, G., Maraschi, L., & Comastri, A. 1998, MNRAS, 301, 451
Ghisellini, G., & Tavecchio, F. 2008, MNRAS, 387, 1669
Ghisellini, G., & Tavecchio, F. 2009, MNRAS, 397, 985
Ghisellini, G., & Tavecchio, F. 2010, MNRAS, 409, 79
Ghisellini, G., Tavecchio, F., Foschini, L., et al. 2010, MNRAS, 402, 497
Ghisellini, G., Tavecchio, F., & Ghirlanda, G. 2009, MNRAS, 399, 2041
Giommi, P., Polenta, G., Lähteenmäki, A., et al. 2012, A&A, 541, 160
Godfrey, L. E. H., & Shabala, S. S. 2013, ApJ, 767, 12
Gu, M., Cao, X., & Jiang, D. 2009, MNRAS, 396, 984
Gu, Q., & Huang, J. 2002, ApJ, 579, 205
Hirotani, K. 2005, ApJ, 619, 73
Ho, L. C. 2008, ARA&A, 46, 475
Hönig, S. F., & Beckert, T. 2007, MNRAS, 380, 1172
Hovatta, T., Valtaoja, E., Tornikoski, M., & Lahteenmaki, A. 2009, A&A, 498, 723
Jorstad, S. G., Marscher, A. P., Larionov, V. M., et al. 2010, ApJ, 715, 362
Kaspi, S., Brandt, W. N., Maoz, D., et al. 2007, ApJ, 659, 997
Kataoka, J., Madejski, G., Sikora, M., et al. 2008, ApJ, 672, 787
Kino, M., Kawakatu, N., & Takahara, F. 2012, ApJ, 751, 101
Krawczynski, H., Hughes, S. B., Horan, D., et al. 2004, ApJ, 601, 151
Kushwaha, P., Sahayanathan, S., & Singh, K. P. 2013, MNRAS, 433, 2380
Laor, A. 2003, ApJ, 590, 86
Lei, W.-H., Wang, D.-X., & Ma, R.-Y. 2005, ApJ, 619, 420
Lei, W.-H., Wang, D.-X., Zou, Y.-C., & Zhang, L. 2008, CHJAA, 8, 404
León-Tavares, J., Valtaoja, E., Giommi, P., et al. 2012, ApJ, 754, 23
León-Tavares, J., Valtaoja, E., Tornikoski, M., et al. 2011, A&A, 532, 146
Li, S.-L., & Cao, X. 2012, ApJ, 753, 24
Liang, E. W., & Liu, H. T. 2003, MNRAS, 340, 632
Liu, H. T., & Bai, J. M. 2006, ApJ, 653, 1089
Liu, Y., & Jiang, D.-R. 2006, ApJ, 637, 669
Mankuzhiyil, N., Ansoldi, S., Persic, M., & Tavecchio, F. 2011, ApJ, 733, 14
Marscher, A. P., & Gear, W. K. 1985, ApJ, 298, 114
Marscher, A. P., Jorstad, S. G., Larionov, V. M., et al. 2010, ApJL, 710, L126
Maraschi, L., Celotti, A., & Ghisellini, G. 1992, ApJ, 397, 5
Maraschi, L., & Tavecchio, F. 2003, ApJ, 593, 667
Mastichiadis, A., & Kirk, J. G. 1997, A&A, 320, 19
Narayan, R., & McClintock, J. E. 2012, MNRAS, 419, 69
Narayan, R., & Yi, I. 1994, ApJL, 428, L13
Narayan, R., & Yi, I. 1995, ApJ, 444, 231
Orienti, M., Koyama, S., D'Ammando, F., et al. 2013, MNRAS, 428, 2418
Pacciani, L., Donnarumma, I., Denney, K. D., et al. 2012, MNRAS, 425, 2015
Padovani, P., & Giommi, P. 1995, ApJ, 444, 567
Paliya, V. S., Stalin, C. S., Shukla, A., & Sahayanathan, S. 2013, ApJ, 768, 52
Panaitescu, A., & Kumar, P. 2001, ApJL, 560, L49
Potter, W. J., & Cotter, G. 2013, MNRAS, 431, 1840
Poutanen, J., & Stern, B. 2010, ApJL, 717, L118
Rafferty, D., McNamara, B., Nulsen, P., & Wise, M. W. 2006, ApJ, 652, 216
Reynolds, C. S., Fabian, A. C., Celotti, A., & Rees, M. J. 1996, MNRAS, 283, 873
Rybicki, G. B., & Lightman, A. P. 1979, Radiative Processes in Astrophysics (New York: Wiley-Interscience), 393
Sambruna, R., Ghisellini, G., Hooper, E., et al. 1999, ApJ, 515, 140
Sari, R., Piran, T., & Narayan, R. 1998, ApJ, 497, 17
Savolainen, T., Homan, D. C., Hovatta, T., et al. 2010, A&A, 512, A24
Shakura, N. I., & Sunyaev, R. A. 1973, A&A, 24, 337
Sikora, M., Begelman, M. C., & Rees, M. J. 1994, ApJ, 421, 153
Sikora, M., & Madejski, G. 2000, ApJ, 534, 109
Sikora, M., Moderski, R., & Madejski, G. 2008, ApJ, 675, 71
Sikora, M., Stawarz, Ł., Moderski, R., et al. 2009, ApJ, 704, 38
Sokolov, A., & Marscher, A. P. 2005, ApJ, 629, 52
Spruit, H. C. 2010, LNP, 794, 233
Tavecchio, F., Maraschi, L., Ghisellini, G., et al. 2007, ApJ, 665, 980
Tavecchio, F., Maraschi, L., Sambruna, R. M., & Urry, C. M. 2000, ApJ, 544, 23
Tavecchio, F., Pacciani, L., Donnarumma, I., et al. 2013, MNRAS, 435, 24
Tran, H. D. 2001, ApJL, 554, L19
Urry, C. M, & Padovani, P. 1995, PASP, 107, 803
Valtonen, M. J., Ciprini, S., & Lehto, H. J. 2012, MNRAS, 427, 77
Vovk, Ie., & Neronov, A. 2013, ApJ, 767, 103
Wang, J.-M., Staubert, R., & Ho, L. C. 2002, ApJ, 579, 554
Wardle, J. F. C., Homan, D. C., Ojha, R., & Roberts, D. H. 1998, Natur, 395, 457
Wehrle, A. E., Marscher, A. P., Jorstad, S. G., et al. 2012, ApJ, 758, 72
Wu, Q., & Cao, X. 2006, PASP, 118, 1098
Wu, Q., Cao, X., Ho, Luis, C., & Wang, D.-X. 2013, ApJ, 770, 31
Wu, Q., Cao, X., & Wang, D. X. 2011, ApJ, 735, 50
Wu, Q., Yuan, F., & Cao, X. 2007, ApJ, 669, 96
Xu, Y.-D., Cao, X., & Wu, Q. 2009, ApJ, 694, 107
Yan, D., Zeng, H., & Zhang, L. 2014, MNRAS, 439, 2933
Zhang, J., Liang, E.-W., Zhang, S.-N., & Bai, J. M. 2012, ApJ, 752, 157
Zhang, J., Sun, X.-N., Liang, E.-W., et al. 2014, ApJ, 788, 104